2019 SECED Conference
Earthquake risk and engineering towards a resilient world
9-10 September 2019, Greenwich, London

UPDATE OF THE UK STOCHASTIC GROUND MOTION MODEL USING A DECADE OF BROADBAND DATA

Andreas RIETBROCK[1] and Benjamin EDWARDS[2]

Abstract: *We present an update to the UK stochastic earthquake ground motion model originally presented by Rietbrock et al. (2013). The update takes advantage of newly available high-quality broadband 3-component data, recorded over the last decade. We estimate M_w for the three largest events by calculating regional moment tensors. Spectral analysis of the data has been performed in order to calibrate the seismological model for use in stochastic simulations. Site-specific attenuation, κ_0, was assessed through the spectral analysis of high-frequency Fourier amplitude spectra (FAS) of larger magnitude UK events (M_L>3.5). Broadband fitting of the FAS was then performed to extend the analysis to low magnitudes (M_L>1.5). We inverted the FAS for source corner frequencies, seismic moments (and magnitudes) and a geometrical spreading function. The average stress parameter based on this analysis was around 1 MPa. In extrapolating to higher magnitude we propose three alternative stress-parameter models[†] (1 MPa rising to 5, 10 and 20MPa above M_w = 4.5) to reflect epistemic uncertainty. The seismological model was implemented in the stochastic ground-motion method framework considering the effects of finite faults. Earthquakes of between M_w = 3 and 7 were simulated over a depth distribution consistent with UK seismicity. Using records at between 1 and 300 km distance a suite of GMPEs was then developed, each based on approximately 126,000 data-points.*

Introduction

This paper documents work commissioned by ARUP, on behalf of Horizon Nuclear Power, and undertaken by the authors to update the existing UK ground motion model (GMM) of Rietbrock *et al.* (2013). The work is carried out within the larger scope of a probabilistic seismic hazard analysis (PSHA) for a nuclear power plant (NPP) site at Wylfa Newydd in the UK (Villani *et al*., 2019, Lubkowski *et al.*, 2019). Within this project, the work presented here has been subject to independent peer review by a panel of experts with oversight by the Office for Nuclear Regulation (ONR). The update to the GMM takes advantage of newly available horizontal ground motion data recorded at the permanent UK national network operated by the British Geological Survey (BGS). As part of this work we have (i) reassessed the source, path and site effects published in Edwards *et al.* (2008) using Q tomography; (ii) developed a ground motion database based on stochastic simulations; and (iii) derived ground motion prediction equations (GMPEs) using the ground motion database.

The UK is classed as a stable continental tectonic region (SCR) and exhibits low seismicity (Delavaud *et al.*, 2012). The largest known UK event occurred in the North Sea at Dogger Bank on 7 June 1931 with M_w 5.8 (M_L 6.1). Since its epicentre was ~100km offshore it caused little damage, although it was widely felt. Several historical earthquakes have also been documented, all of which are thought to be between M_w 5 – 6 (Musson, 1996). The limited records of these events makes reliable magnitude estimation difficult. However, maximum magnitudes (M_{max}) considered for probabilistic seismic hazard analyses (PSHAs) in the UK are typically 5.5 – 7 (Musson and Sargeant, 2007; Woessner *et al*., 2015).

As a result of the low seismicity in the UK there are no strong-motion earthquake records available with which to calibrate a local ground motion prediction equation valid up to M_{max}. Furthermore, using ground motion prediction equations developed in active shallow crustal regions (ASCRs), such as those developed as part of the Next Generation (NGA) West projects, is not straightforward in SCRs. In these cases, adjustments are typically required to account for differing geological conditions (Edwards *et al.*, 2016). In order to address this issue a stochastic earthquake GMM was presented by Rietbrock *et al.*, (2013). The model was calibrated by considering source, path and site parameters determined by Edwards et al. (2008), who analysed available weak-motion data available at the time (single component vertical records). The work

[1] Prof, Karlsruhe Institute of Technology, Karlsruhe, Germany
[2] Dr, University of Liverpool, Liverpool, UK, ben.edwards@liverpool.ac.uk
[†] Electronic Appendix

presented here seeks to update that model in light of newly available high-quality broadband 3-component data, recorded over the last decade by the BGS.

Ground-motion Database

Recorded earthquake waveforms were obtained from the BGS. Two separate datasets were defined: (1) recordings of all events with $M_L \geq 2.0$; and (2) recordings of all located events (without magnitude threshold) where station WPS (near the Wylfa Newydd NPP site) was triggered. The two were combined to form the ground-motion dataset used in this work. The dataset includes waveform and event location data for 273 earthquakes, comprising 190 earthquakes with $M_L \geq 2$ and 83 additional events with $M_L < 2$ recorded at station WPS. For the 273 events all available waveform data from the BGS permanent broadband seismic network, event location solutions and picked P- and S-wave arrivals were provided by the BGS. For all waveforms provided we have performed signal-to-noise ratio (SNR) analysis to select high-quality recordings and to define usable frequencies. Signal windows were selected by initially extracting a window of 50 s, starting 5 s before the S-wave arrival and ending 45 s after. The S-wave time was either a manually picked arrival, or if unavailable, estimated based on a P-wave pick and a v_p:v_s ratio of 1.73. The signal window was then reduced to provide the 5-95% significant shaking duration, which is consistent with random vibration theory (Boore and Thompson, 2014). 4 s noise windows were taken from the start of the waveform (before the P-wave arrival). Signal and noise windows were then transformed to the Fourier domain using an adaptive weight multi-taper algorithm. Noise FAS are increased such that the lowermost (f < ~0.1 Hz) and uppermost frequencies (f > ~45 Hz) are coincident with signal amplitudes to avoid issues related to uncertainty of low-frequency FAS amplitudes (too few wavelengths in signal) and sensor tilt. Finally, the resulting FAS were corrected for the instrument response.

SNR analysis was used to define for each recording the continuous signal bandwidth (between f_{low} and f_{high}) that exceeded the noise estimate by a factor 2.5. The minimum requirement for data fit in the linear frequency domain was f_{low} < 5Hz and f_{high} > 15 Hz. FAS at frequencies between the record-specific SNR limits were then used in subsequent inversions for spectral decay [defined by κ (Anderson and Hough, 1984)]. For subsequent inversions of corner frequency and signal moment, we instead required f_{high} > 10 Hz with the constraint that f_{high}/f_{low} > 10 to ensure adequate bandwidth in the log-space. Due to different minimum bandwidth criteria, the final waveform database, after SNR analysis consisted of 1187 recordings from 236 events for the determination of κ and 884 records of 182 events for the determination of seismic moment and source corner frequencies. A distribution of the data (passing the linear-frequency SNR test) in terms of magnitude, distance, depth and frequency content is shown in Figure 1.

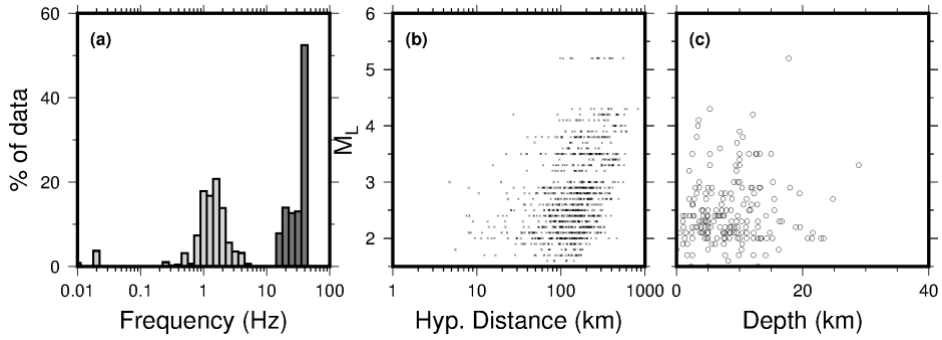

Figure 1. Plot of available data in terms of (a) frequency content [grey – lower limit, dark grey – upper limit with acceptable SNR] and magnitude versus (b) distance and (c) depth.

Broadband fitting of Acceleration FAS

Determination of κ values

FAS were fit using least-squares minimisation following the approach detailed in Edwards *et al*. (2008). The Fourier velocity spectrum is given by:

$$\Omega_{ij}(f,r) = 2\pi f E_i(f, f_{ci}) B_{ij}(f, \kappa_{ij}) S_{ij} T_j I_j(f) \quad (1)$$

where E is the (Brune, 1970) source model for event *i* with a defining corner-frequency f_c. *B* is the attenuation along the ray path to site *j*:

$$B_{ij}(f) = e^{-\pi f \kappa_{ij}} \tag{2}$$

with κ the frequency independent whole path attenuation operator defined by:

$$\kappa_{ij} = \frac{t_{ij}}{Q_{ij}}. \tag{3}$$

t is the travel time and *Q* is the path dependent dimensionless quality factor. It should be noted that due to the relatively long window lengths used (encapsulating the duration of significant shaking) the degree of attenuation may vary at different points in the window due to different paths and corresponding travel times of the individual phases. In this case the attenuation parameter, κ, obtained from inversion will describe the average attenuation over all the travel paths in the signal window. *S* is the frequency independent amplitude decay with distance and *T* is the source to site amplification factor (including the 'rock-amplification' due to increasing velocity with depth) at the recording station. Finally, *I* is the instrument response function. This inversion problem is solved by searching for three parameters: (i) the source corner frequency, f_c, (common to each event), (ii) the signal moment (which accommodates all frequency-independent effects, such as *S*, and (iii) κ values (specific to each FAS). The geometrical mean of the horizontal FAS are initially fit in the log-velocity, linear-frequency space to focus on high frequencies [similar to the approach of Anderson and Hough (1984)]. Note the use of velocity or acceleration here is accounted for simply by $2\pi f$ in the FAS. An example of the spectral fits is given in Figure 2 along with a comparison of the κ values obtained using this method and those from only fitting the high-frequency data (f > 10Hz) for larger (M_L > 3.5).

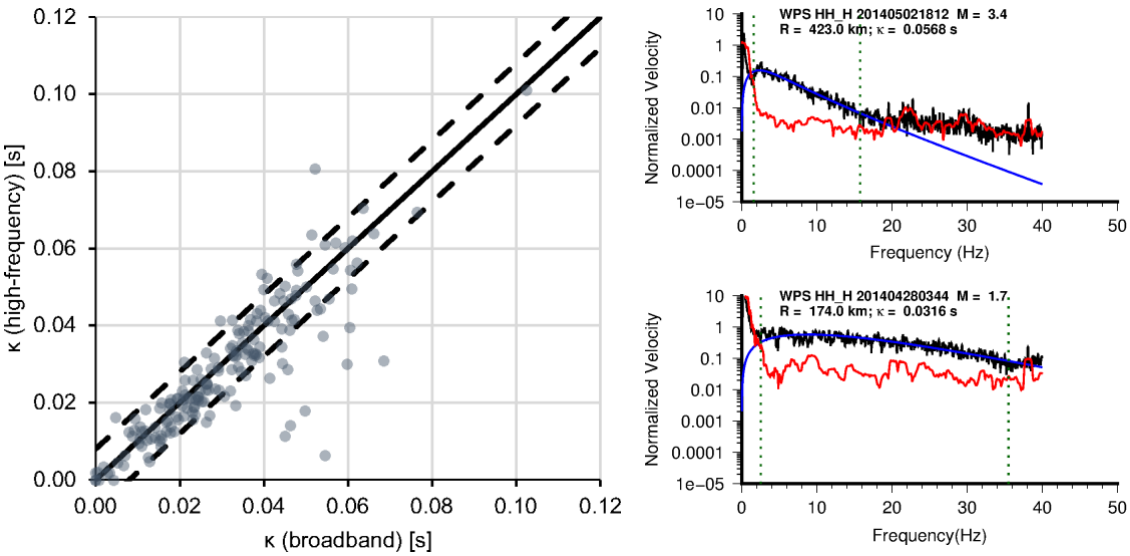

Figure 2. Left: comparison of a subset of κ values determined using a high frequency fit with those from the broadband spectral fitting (where both available). Epistemic uncertainty of +/- 0.008s (Edwards et al., 2015) is indicated by the dashed lines. Right: Example FAS of velocity recorded at site WPS fit in the lin-log space. Black: S-wave signal; red: noise; blue: modelled FAS; vertical lines: fitting limits. All FAS are normalised by the peak modelled FAS value.

Inversion for 1D Q Model and Forward Modelling of κ

Following the determination of path κ, the values are used in a tomographic inversion for the 1D Q structure (Rietbrock, 2001). In total 1159 κ value observations from 229 earthquakes recorded at 55 seismic stations were used. The inversion is based on ray-tracing velocity tomography with iterative linearization modified to calculate Q. To be consistent with station dependent κ, the inversion algorithm was modified to incorporate a positivity constraint for station specific κ_0 values. Optimum damping was chosen by simultaneously minimizing model and data variance to be able to derive the best model without over fitting noise.

Table 1 gives the depth-dependent Q model in comparison to the values which were obtained by Edwards *et al*. (2008). As can be seen the Q models from the two studies are broadly comparable,

taking into account that Edwards *et al*. (2008) used vertical component short period S-wave data whereas this study only used horizontal component broadband data. The new model indicates somewhat stronger damping (lower Q) in the upper layers, which combined with the positive κ_0 constraint (which was not used for the previous model), will lead to stronger anelastic path attenuation. The inverted Q model together with corresponding station dependent κ_0 values were used to calculate synthetic path κ values which are used in the subsequent inversion step to estimate source corner frequency and signal moments.

Depth (km)	Q (Edwards et al. 2008)	Q (this study)
2.5	990	720
20	1000	1005
34	5500	4875

Table 1. Obtained attenuation model in comparison to Edwards et al. (2008).

Inversion for Geometrical Decay

The signal moment (long-period spectral displacement plateau) can be split into contributions from the source, path and site. The signal moment is given by:

$$\hat{\Omega}_{ij} = \Psi_i A_j S_{ij}(r, r_{0\ldots n-1}, \lambda_{1\ldots n}) \quad (4)$$

Geometrical decay S with constant exponential decay ($\lambda_{1..n}$) between distances $r_{0..n-1}$ is:

$$S_{ij}(r, r_{0\ldots n-1}, \lambda_{1\ldots n}) = \begin{cases} \left(\frac{r_0}{r}\right)^{\lambda_1} & r \le r_1 \\ S(r_1)\left(\frac{r_1}{r}\right)^{\lambda_2} & r_1 \le r \le r_2 \\ \vdots & \vdots \\ S(r_n)\left(\frac{r_n}{r}\right)^{\lambda_n} & r \ge r_n \end{cases} \quad (5)$$

A_j is the site amplification parameter independent of frequency, and Ψ_i is the amplitude of the spectral displacement plateau at the source at the source (i.e., proportional to the time-integral of the moment-rate function). Seismic moments, M_0 (in SI units), can be calculated using the following equation:

$$M_0 = \frac{\Psi\ v^3 \rho r_0 4\pi}{F\Theta_{\lambda\Phi}}, \quad (6)$$

(Brune, 1970) where $\Theta_{\lambda\Phi}$ is the average radiation pattern ($\Theta_{\lambda\Phi}$=0.55 for S waves at local to regional distances), v is the velocity at the source (3500 m/s), F is the free surface amplification (2.0 for normally incident SH waves), ρ is the average crustal density (2800 kgm^{-3}) and r_0 is the fault radius (as used in Eq. 5).

A general least-squares inversion is used to obtain the geometrical spreading function, site amplification and moment magnitudes [see Edwards *et al.* (2008) for details of the approach]. We invert for a new geometrical spreading model and constrain the inversion by fixing the moment tensor derived M_w values of the 2008 Market Rasen (M_w 4.5), 2014 Bristol Channel (M_w 3.7) and 2015 Ramsgate (M_w 3.7) earthquakes. This is a change to the approach used by Edwards *et al.* (2008) who assumed unitary average amplification across the network (potentially underestimating site effects). As in Edwards *et al.* (2008) the initial decay rate was fixed to λ_1=1.0 as there still exists a trade-off between site amplification and the rate of initial decay due to the limited quantity of data recorded at R < 50 km in the UK. The same segmentation distances as previously were used (r_0=1 km, r_1=50 km, r_2=100 km). We find λ_2=-0.11 and λ_3=2.01. This is not dissimilar to the model originally derived in the previous analysis by Edwards *et al.* (2008). The decay at R > 100km is somewhat less – possibly due to stronger surface wave contributions on the horizontal component.

Figure 3 shows that the trend of M_L:M_w closely follows that of Grünthal *et al.* (2009). The geometrical spreading function is also shown in Figure 3. No obvious misfit trends are apparent either in magnitude or distance. Beyond 300km, the decay further steepens, but this is not considered important to capture in the model since the hazard will be not influenced by such scenarios. We note that the steep decay at R > 100 km may be capturing frequency dependent Q, which is not considered in this model. Alternatively, a vertical and lateral varying velocity model could also cause the steep decay at R > 100 km.

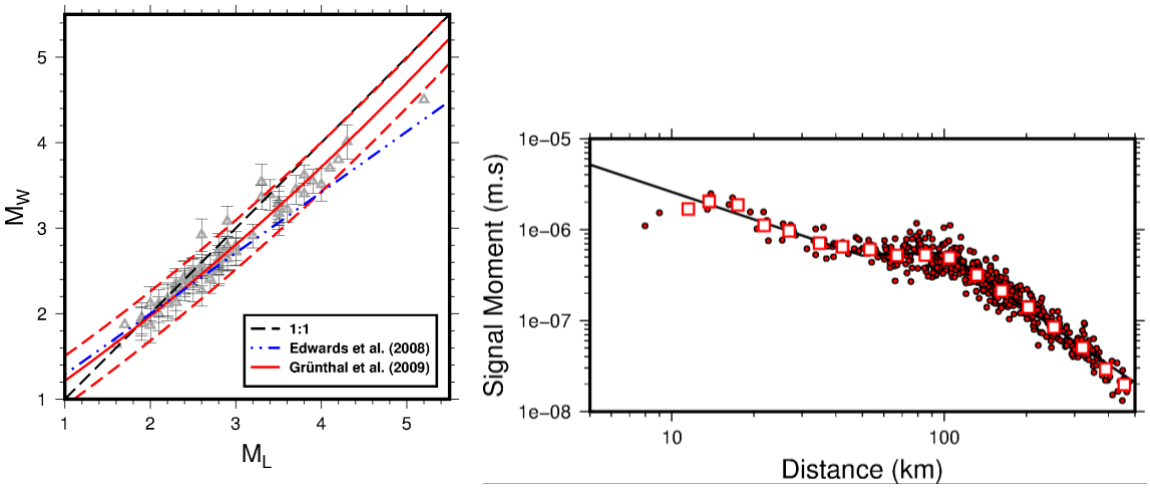

Figure 3. Left: moment magnitudes plotted against local magnitudes. The standard error of the M_w values is indicated where available. The blue line indicates the M_w:M_L model presented by Edwards et al. (2008). The red line shows the M_w:M_L model and standard deviation (dashed red line) of Grünthal et al. (2009). Right: signal moments – normalised to a M_w3 event at a reference site – plotted against distance. The geometrical spreading model is shown by the grey line. Binned average values are shown by the squares.

Stress Parameter for UK Events

Stress parameter is an important seismological input, particularly for large events as it controls, for a given magnitude, the level of shaking at a wide range of oscillator periods. The stress-parameter can be obtained from the source parameters derived during spectral analysis using:

$$\Delta\sigma = \mathrm{M}_0 \left(\frac{f_c}{0.4906\beta} \right)^3 \tag{7}$$

(Boore, 2003) where β is the near-source velocity (assumed to be 3500m/s). The stress parameters obtained for the UK data are shown in Figure 4. The log-average stress parameter was 0.9 MPa (9 bars) with a standard deviation of +/- 0.56 in log10 units. From M_w= 3 and up the results indicate that the stress parameter increases, from average values less than 1 MPa up to the largest event in our dataset, Market Rasen, has a stress parameter of 6.1 MPa. However – this might be a sampling issue, with few events with M_w > 3.

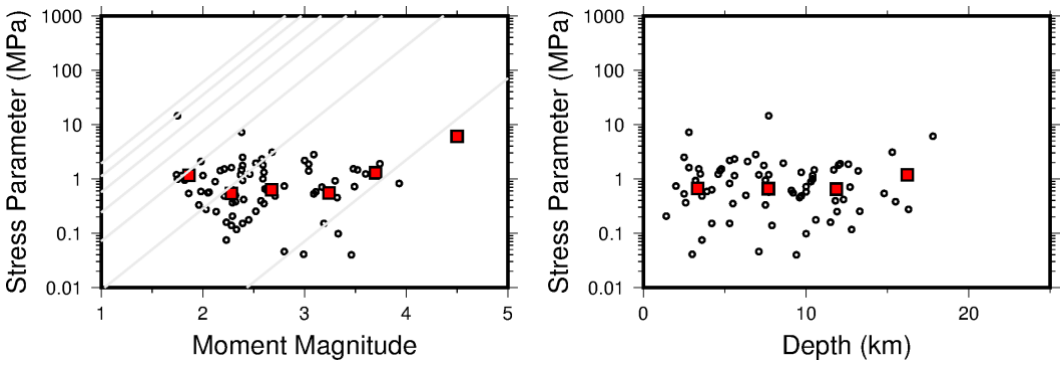

Figure 4: Stress parameter plotted against (left) M_w and (right) depth. Squares indicate bin-average values. Grey lines in the left panel indicate constant corner frequencies (from bottom right to top left: 1, 5, 10, 15, 20, 25 and 30 Hz)

Shaking Durations

The duration model T_D used in SMSIM (Boore, 2003) is comprised of a source (T_S) and path (T_P) component:

$$T_D = T_S + T_P \tag{8}$$

The source component can be assumed to be related to the source corner-frequency (or frequencies if multiple corner source models are used). We assume that the source component to duration is given by $1/f_c$, consistent with the strong-motion duration model of Kempton and Stewart (2006). The path component to the duration model aims to capture the dispersion of the wavefield due to scattering as we get further away from the source. It is typically measured using some form of 'significant duration'. There are numerous ways in which to define and measure significant duration. We adopt the recommendation of Boore and Thompson (2014) who state that the 5-95% arias intensity (denoted D_{95}) is compatible with SMSIM. Boore and Thompson (2014) recommended that noise issues could be avoided by estimating D_{95} using:

$$D'_{95} = 2(D_{80} - D_{20}) \tag{9}$$

where D_x denotes the 5-x% arias intensity which may be less sensitive to noise. We find durations consistent with the model used by Rietbrock et al. (2013), which is therefore adopted here.

Stochastic simulations: methodology

The stochastic method of Boore (2003) is used to simulate ground-motion in terms of peak ground acceleration (PGA) and 5% damped response pseudo-spectral acceleration (PSA) at periods between 0.01 and 5s. We closely follow Rietbrock *et al.* (2013) in terms of preparing the input parameters for the stochastic simulations, updating the mean values and uncertainties based on the new seismological model. As the stochastic method relies on the knowledge of the expected FAS of an earthquake with a given M_w at a certain distance it is essential to incorporate as much knowledge as possible of the variances and the interdependencies of the model parameters.

Model parameters

The input parameters for the stochastic simulations undertaken in the present study are summarised in Table 2. As pointed out in Rietbrock *et al.* (2013) one of the predominant source of uncertainties is the limited information available regarding the values of the stress parameter, which controls the level of the high-frequency acceleration plateau in the ω^2 Brune model (1970). Although we could constrain the average stress parameter to 1 MPa in the magnitude range between 2-3 the lack of higher magnitude recordings prevents a direct estimation of the stress parameter of the UK for larger magnitude events ($M_w > 5$). Rietbrock *et al.* (2013) proposed two different stress parameter models. The first model assumed a constant stress parameter of 1 MPa, while the second used a magnitude dependent stress parameter. The latter incorporated a linear increase in the stress parameter between 0.7 MPa at M_w=3 and 10 MPa at M_w=4.5, which was based on published values [see Figure 2 in Rietbrock *et al.* (2013)]. In order to explore the uncertainty associated with the scaling of the stress parameter in the UK, we evaluated alternative models for the 'magnitude-dependent' case. In all cases, the form follows Rietbrock *et al*. (2013) with a median stress parameter of 1 MPa below M_w=3 and 5, 10 or 20 MPa above M_w=4.5.

Model Parameter Variability

For each of the parameters defining the expected FAS, overall values of variability are defined (Table 2). However, it is known that these parameters are not independent in terms of modelling uncertainty, and therefore it is essential to take into account the covariance between parameters during the simulation stage. We define two sources of variability in the model parameters: (i) the uncertainty introduced due to the non-unique modelling of the Fourier spectra, which are known to be covariate; (ii) the uncertainty due to model simplicity, which contributes to the epistemic uncertainty. For the interpretation and simulations, it is important to take into account these model parameter interdependencies. Based on a bootstrap approach and a large weak motion data set for the UK, Edwards *et al.* (2008) estimated the covariance matrix for whole path attenuation operator κ (termed *t** in their work), the source corner frequency f_c, and the spectral displacement plateau value Ψ (Table 3). For the simulations, the use of the covariance matrix's Cholesky decomposition, L, is required (Table 3), where:

$$C = LL^T. \tag{10}$$

Table 2. Overview of Parameter Distributions Used to Define the Expected FAS of UK Events in the stochastic simulations.

Parameter	***Model***
Focal Depth	Discrete distribution 5 km [weight=0.1], 10 km [w=0.25], 15 km [w=0.4] and 20 km [w=0.25]
Stress parameter Δσ	Lognormal distribution: μ=1.0 MPa for $M_w \leq 3.0$; μ=10.0 MPa for $M_w \geq 4{:}5$; standard-deviation $\log_{10}$ σ=0.54 at $M_w < 3.0$; σ=0.40 ($\log_{10}$) for $M_w \geq 4.5$; linear interpolation of log10 Δσ between M_w 3.0 and M_w 4.5. linear interpolation between nodes.
Attenuation at depth D:	Q_D=720 at D = 2.5 km Q_D=1005 at D = 20km Q_D=4875 at D = 34km Uncertainty controlled by κ error 2.66×10^{-4} s
Local variation of attenuation: Δκ	Truncated normal distribution μ=0.005 s, σ=0.008 s Min/Max: 0.000/0.025 s
Geometrical spreading	$1/R^{1.00}$ for $R_{hyp} \leq 50$ km $1/R^{-0.11}$ for $50 < R_{hyp} \leq 100$ km $1/R^{2.01}$ for $R_{hyp} > 100$ km
Variability of spectral plateau	Truncated normal distribution μ=0.0, σ=0.2675 ($\log_{10}$) Min/Max: −0.57/0.45
Duration of shaking: T_d	0 + $1/f_c$ s at 0 km 7.0 + $1/f_c$ s at 60 km 7.0 $1/f_c$ s at 150 km 37 $1/f_c$ s at 400 km
Rock amplification A(f)	*Quarter-wavelength approximation of amplification from generic UK V_S profile beneath a layer of Vs=2600m/s with a thickness of 30m.*

Table 3. Covariance Matrix (C) and Cholesky Decomposition (L) of the FAS model Parameters

C	**log(ΔΨ)**	**Log(Δκ)**	**Log(Δfc)**
log(ΔΨ)	0.005354	__	__
Log(Δκ)	0.001909	0.004802	__
Log(Δfc)	-0.002866	0.001355	0.005112

L	**log(ΔΨ)**	**Log(Δt*)**	**Log(Δfc)**
log(ΔΨ)	0.073171	__	__
Log(Δκ)	0.02609	0.064198	__
Log(Δfc)	-0.039169	0.037025	0.046979

The procedure for simulating the n^{th} spectrum is as follows. First we compute the normalised uncorrelated random deviation, $P_{log,x}(\mu,\sigma)$, due to modelling uncertainty of each of the defining spectral parameters, the spectral plateau ($\Delta\Psi_M$), whole path attenuation ($\Delta\kappa_M$), and source corner frequency (Δfc_M). This is achieved by taking a random value from the lognormal distribution with zero mean and unit standard deviation. $\Delta\Psi_M$ is used as the reference deviation, such that the covariate factorial deviations are then given by:

$$log(\Delta\Psi_M) = L_{11}P_{log,\Delta\Psi}(0,1), \quad (11)$$

$$log(\Delta\kappa_M) = L_{21}P_{log,\Delta\Psi}(0,1) + L_{22}P_{log,\Delta\kappa}(0,1),$$

$$log(\Delta f_{c_M}) = L_{31}P_{log,\Delta\Psi}(0,1) + L_{32}P_{log,\Delta\kappa}(0,1) + L_{33}P_{log,\Delta fc}(0,1),$$

where the uncorrelated standard deviations of $\Delta\Psi_M$, $\Delta\kappa_M$, and Δfc_M are given by L_{11}, L_{22}, and L_{33}, respectively. Δfc_M is used to calculate $\Delta(\Delta\sigma)_M$ using:

$$f_c = 0.4906\beta\left(\frac{\Delta\sigma}{M_0}\right)^{\frac{1}{3}} \quad (12)$$

with Δσ in MPa. Finally, the remaining uncorrelated deviations are applied (Table 2).

Modelling considerations for updated UK GMPE

The stochastic simulation software SMSIM—Fortran Programs for Simulating Ground Motions from Earthquakes (www.daveboore.com, accessed 29 August 2012) was used for the stochastic simulations. For each ground-motion parameter, 126,000 ground motion values were calculated, corresponding to 9000 simulated earthquake events. For each event, M_w and hypocentral depth were fixed, and one realization of the stochastic parameter sampling was drawn from the appropriate probability distribution, including consideration of covariance as described above. M_w were varied from 3.0 to 7.0 in 0.5 unit increments, and, following Musson and Sargeant (2007),

the hypocentral depths considered were 5, 10, 15, and 20 km, weighted to reflect the observed distribution in the UK. Ground motions were computed for a linear array of 14 receivers located at fixed epicentral distances of 1, 2, 5, 10, 15, 20, 30, 40, 50, 60, 70, 80, 90, 120, 150, 200, 250, and 300 km. We account for finite-fault effects based on Wells and Coppersmith (1994) following the geometrical approach detailed in Rietbrock *et al.* (2013).

Parametric form of the updated UK GMPE model

The following functional form was fitted to the results of the numerical simulations:

$$\log_{10}(Y) = c_1 + c_2 M_w + c_3 M_w^2 + (c_4 + c_5 M_w) F_0 + (c_6 + c_7 M_w) F_1 + (c_8 + c_9 M_w) F_2 + c_{10} R \quad (13)$$

$$R = \sqrt{R_{jb}^2 + c_{11}^2}\,;\; F_0 = \begin{cases} \log_{10}\left(\frac{r_0}{R}\right) & for\ R \le r_0 \\ 0 & for\ R > r_0 \end{cases};\; F_1 = \begin{cases} \log_{10}\left(\frac{R}{1.0}\right) & for\ R \le r_1 \\ \log_{10}\left(\frac{r_1}{1.0}\right) & for\ R > r_1 \end{cases};\; F_2 = \begin{cases} 0 & for\ R \le r_2 \\ \log_{10}\left(\frac{R}{r_2}\right) & for\ R > r_2 \end{cases}$$

with r_0=10 km, r_1=50 km and r_2=100 km. In view of the regular spacing and large number of data points to include in the regression (N=126,000), the choice of the regression procedure is not expected to significantly affect the results, unlike for empirical data sets. The regressions have therefore been carried out using a non-linear least-squares procedure, with an ordinary least-squares solution to determine initial estimates. The best-fitting GMPE coefficients are summarized in Table 4 for the 10 MPa stress parameter model and in the electronic appendix†.

Comparison with Recent Data

Residual analyses were undertaken with data from recent moderate (M_w > 3.5) events in addition to macroseismic intensity data and were found to provide unbiased predictions (Villani et al., 2019). LLH testing showed the updated GMPE to consistently out-perform other candidate GMPEs. A comparison with the most recent moderate event in Swansea, 2018 (M_w=4.3), which was not included in the GMM calibration, is shown in Figure 5. While unfortunately the data are only available above 50 km, the updated GMPE clearly does a better job at predicting the median PGA than both the previous UK GMPE and other global GMPEs.

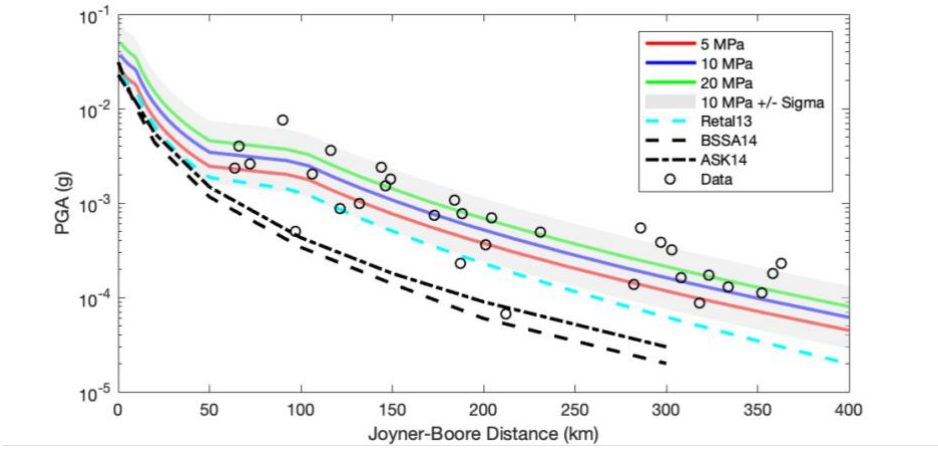

Figure 5. Comparison of predicted PGA for the 2018 Swansea earthquake (M_w=4.3) with those of the GMPE presented here, the model of Rietbrock et al. (2013) and Boore et al. (2014) and Abrahamson et al. (2014). Predictions are shown for the 10 MPa model in addition to two alternative models with 5 and 20 MPa respectively.

Conclusion

The UK specific GMPE presented herein provides an update to the Rietbrock *et al.* (2013) GMM through calibration of a stochastic earthquake ground motion model using a decade of new data. The model was developed within the framework of a large-scale PSHA project for the Wylfa Newydd NPP and subject to independent peer review. The seismological model and simulation framework proposed here offers the ability to predict either UK calibrated motions (Eq. 13, Table 4, Electronic Appendix†) or to tailor simulations (Tables 2, 3) using site-specific velocity and damping models. The latter provides application-specific predictions to reduce the uncertainty associated with host-to-target GMM adjustment, as used in the Wylfa Newydd NPP PSHA.

† Electronic Appendix

Table 4. UK GMPE coefficients derived from the simulations using the 10 MPa Stress Parameter for $M_w > 4.5$

Frequency	Period	C_1	C_2	C_3	C_4	C_5	C_6	C_7	C_8	C_9	C_{10}	C_{11}	σ_T	σ_B	σ_W
--	PGV	-4.4578	1.6540	-0.1044	-1.6308	0.2082	-1.6465	0.1568	-2.3547	0.0676	-0.000991	2.8899	0.2704	0.2199	0.1573
--	PGA	-2.1780	1.6355	-0.1241	-1.8303	0.2165	-1.8318	0.1622	-1.9899	0.0678	-0.002073	2.3460	0.3323	0.2858	0.1695
33.33	0.03	-1.3946	1.5566	-0.1210	-2.1447	0.2324	-2.0955	0.1777	-1.7240	0.0891	-0.003079	1.5613	0.3642	0.2951	0.2133
25.00	0.04	-1.5298	1.5684	-0.1181	-1.8704	0.1906	-1.8175	0.1420	-1.5458	0.0827	-0.003522	1.4637	0.3573	0.2977	0.1975
20.00	0.05	-1.6747	1.5876	-0.1178	-1.7218	0.1719	-1.6779	0.1258	-1.5486	0.0695	-0.003350	1.5137	0.3506	0.2976	0.1853
16.67	0.06	-1.8507	1.6171	-0.1187	-1.5996	0.1587	-1.5637	0.1136	-1.6102	0.0560	-0.002996	1.6318	0.3422	0.2959	0.1718
12.50	0.08	-2.0520	1.6568	-0.1209	-1.5126	0.1517	-1.4804	0.1057	-1.7039	0.0458	-0.002586	1.8079	0.3336	0.2928	0.1598
10.00	0.10	-2.3048	1.7127	-0.1246	-1.4463	0.1480	-1.4141	0.1000	-1.8096	0.0382	-0.002172	2.0171	0.3250	0.2880	0.1506
8.33	0.12	-2.5981	1.7821	-0.1295	-1.3958	0.1454	-1.3622	0.0956	-1.9028	0.0331	-0.001822	2.1704	0.3174	0.2821	0.1454
6.25	0.16	-2.9711	1.8735	-0.1360	-1.3507	0.1428	-1.3141	0.0915	-1.9872	0.0290	-0.001508	2.2948	0.3097	0.2745	0.1433
5.00	0.20	-3.4163	1.9839	-0.1439	-1.3080	0.1393	-1.2687	0.0872	-2.0567	0.0256	-0.001243	2.3514	0.3023	0.2657	0.1441
4.00	0.25	-3.9043	2.1039	-0.1522	-1.2667	0.1347	-1.2260	0.0829	-2.1103	0.0228	-0.001030	2.3495	0.2954	0.2563	0.1470
3.23	0.31	-4.4356	2.2302	-0.1606	-1.2230	0.1286	-1.1838	0.0783	-2.1517	0.0202	-0.000850	2.2892	0.2889	0.2462	0.1512
2.50	0.40	-4.9975	2.3558	-0.1683	-1.1762	0.1213	-1.1419	0.0736	-2.1841	0.0178	-0.000694	2.1896	0.2827	0.2355	0.1563
2.00	0.50	-5.5468	2.4664	-0.1741	-1.1287	0.1135	-1.1038	0.0693	-2.2080	0.0155	-0.000560	2.0648	0.2770	0.2248	0.1618
1.59	0.63	-6.0465	2.5499	-0.1771	-1.0857	0.1067	-1.0742	0.0663	-2.2253	0.0133	-0.000442	1.9685	0.2719	0.2144	0.1673
1.27	0.79	-6.4705	2.5968	-0.1765	-1.0512	0.1016	-1.0584	0.0655	-2.2384	0.0115	-0.000334	1.8968	0.2676	0.2044	0.1726
1.00	1.00	-6.7771	2.5981	-0.1719	-1.0343	0.1002	-1.0642	0.0681	-2.2491	0.0102	-0.000239	1.8893	0.2640	0.1954	0.1775
0.80	1.25	-6.9495	2.5538	-0.1637	-1.0411	0.1032	-1.0957	0.0748	-2.2593	0.0101	-0.000157	1.9356	0.2610	0.1872	0.1819
0.63	1.59	-6.9977	2.4597	-0.1513	-1.0802	0.1121	-1.1604	0.0866	-2.2724	0.0117	-0.000086	2.0388	0.2580	0.1787	0.1862
0.50	2.00	-6.9298	2.3348	-0.1370	-1.1486	0.1257	-1.2477	0.1018	-2.2897	0.0158	-0.000043	2.1604	0.2550	0.1703	0.1898
0.40	2.50	-6.7909	2.1932	-0.1220	-1.2383	0.1424	-1.3473	0.1184	-2.3139	0.0230	-0.000029	2.2903	0.2517	0.1616	0.1930
0.32	3.13	-6.6206	2.0449	-0.1069	-1.3397	0.1604	-1.4492	0.1350	-2.3503	0.0340	-0.000047	2.4199	0.2480	0.1523	0.1957
0.25	4.00	-6.4512	1.893	-0.0918	-1.4444	0.1782	-1.5462	0.1501	-2.4088	0.0503	-0.000098	2.5430	0.2440	0.1423	0.1982
0.20	5.00	-6.3504	1.7758	-0.0801	-1.5184	0.1896	-1.6103	0.1596	-2.4808	0.0678	-0.000161	2.6018	0.2407	0.1339	0.2001

Acknowledgements

This work was funded by Horizon Nuclear through Arup. We are grateful to numerous individuals for discussions during the development of the model, in particular: Manuela Villani, Rory McCully, Ziggy Lubkowski (Arup) and Martin Walsh and Tim Courtney (Horizon Nuclear). We extend thanks to the independent peer review panel who provided comments and feedback (in particular Willy Aspinall and Gordon Woo) in addition to ONR (Julian Bommer and Richard Fowler).

References

Abrahamson NA, Silva WJ and Kamai R (2014), Summary of the ASK14 Ground Motion Relation for Active Crustal Regions, *Earthq Spectra*, 30: 1025-1055.

Anderson JG and Hough SE (1984), A Model for the Shape of the Fourier Amplitude Spectrum of Acceleration at High-Frequencies, *Bull Seismol Soc Am*, 74: 1969-1993.

Boore DM (2003), Simulation of Ground Motion Using the Stochastic Method, *Pure and Applied Geophys* 160: 635-676.

Boore DM and Thompson EM (2014), Path Durations for Use in the Stochastic‐Method Simulation of Ground Motions, *B Seismol Soc Am*, 104: 2541-2552.

Boore DM, Stewart JP, *et al*. (2014), NGA-West2 Equations for predicting PGA, PGV, and 5% Damped PSA for Shallow Crustal Earthquakes, *Earthq Spectra*, 30: 1057-1085.

Brune, JN (1970), Tectonic Stress and Spectra of Seismic Shear Waves from Earthquakes, *J Geophys Res,* 75: 4997-5009.

Delavaud E, Cotton F, *et al.* (2012), Toward a Ground-Motion Logic Tree for Probabilistic Seismic Hazard Assessment in Europe, *J of Seismol*, doi:10.1007/s10950-012-9281-z.

Edwards B, Rietbrock A, Bommer JJ and Baptie B (2008), The Acquisition of Source, Path, and Site Effects from Microearthquake Recordings Using Q Tomography: Application to the United Kingdom, *B Seismol Soc Am*, doi:10.1785/0120070127.

Edwards B, Ktenidou O-J, Cotton F, *et al.* (2015), Epistemic Uncertainty and Limitations of the κ0 model for Near-surface Attenuation at Hard Rock Sites, *Geophys J Intl*, doi:10.1093/gji/ggv222.

Edwards B, Cauzzi C, Danciu L and Fäh D (2016), Region-Specific Assessment, Adjustment and Weighting of Ground Motion Prediction Models: Application to the 2015 Swiss Seismic Hazard Maps, *B Seismol Soc Am*, doi:10.1785/0120150367.

Grünthal G, Stromeyer D and Wahlstrom R (2009), Harmonization Check of M_w within the Central, Northern, and Northwestern European Earthquake Catalogue (CENEC), *J Seismol,* doi: 10.1007/s10950-009-9154-2.

Kempton JJ and Stewart JP (2006), Prediction Equations for Significant Duration of Earthquake Ground Motions Considering Site and Near-Source Effects, *Earthq Spectra*, 22: 985-1013.

Lubkowski Z, Free M, Musson R, *et al*. (2019), Seismic Hazard Assessment for the Wylfa Newydd Nuclear Power Plant, *this issue*.

Musson R (1996). The Seismicity of the British Isles, A Geophys, doi:10.4401/ag-3982.

Musson R and Sargeant S (2007), Eurocode 8 Seismic Hazard Zoning Maps for the UK. British Geological Survey technical report, 70 pp.

Rietbrock A (2001), P-wave Attenuation Structure in the Fault Area of the 1995 Kobe Earthquake, *J. Geophys. Res.*, 106, 4141-4154.

Rietbrock A, Strasser F and Edwards B (2013), A Stochastic Earthquake Ground‐Motion Prediction Model for the United Kingdom, *B Seismol Soc Am*, 103: 57-77.

Villani M, Polidoro B, McCully R, *et al*. (2019), A Selection of GMPEs for the United Kingdom based on Instrumental and Macroseismic Datasets. Submitted to *B Seismol Soc Am*.

Wells DL and Coppersmith KJ (1994), New Empirical Relationships among Magnitude, Rupture Length, Rupture Width, Rupture Area, and Surface Displacement, *B Seismol Soc* Am 84: 974-1002.

Woessner J, Laurentiu D, Giardini D, *et al*. (2015), The 2013 European Seismic Hazard Model: Key Components and Results, B Earthq Eng 13: 3553-3596.